SLAC-PUB-1962
U.C.S.C 77-061
June 1977
(T/E)

HADRON DISTRIBUTIONS IN A QUARK-PARTON MODEL*

Abraham Seiden

University of California
Santa Cruz, California

and

Stanford Linear Accelerator Center
Stanford, California

Abstract

We present distributions in longitudinal and transverse momentum for hadrons produced in various deep inelastic processes for a particular picture of quark dressing. The sensitivity of various parameters in the model to presently available data is explored. Predictions are also made for the correlations expected in proton-proton scattering events which yield a high transverse momentum pion or kaon, assuming that these originate from a similar quark dressing process.

(Submitted to Nuclear Physics B)

---

*Supported in part by the Energy Research and Development Administration.

I. INTRODUCTION

We present in this paper calculations in a specific quark fragmentation model detailed in Ref. 1. The goal of the paper is, first, to include in a simple way transverse momentum in the quark dressing calculation, allowing further comparisons of the model to recently available data. Second, we make several predictions for the expected particle density accompanying a high transverse momentum meson produced in proton-proton collisions. The distributions predicted have been chosen because they may be measured in the near future, allowing a good test of the hypothesis that quarks are the parents of high transverse momentum mesons. We summarize briefly below the model used throughout this paper. Further details, and, in particular, the motivation behind the numbers used in the model, can be found in Ref. 1.

(1) A deep inelastic process yields a quark isolated in phase space[2].

(2) The hadrons materializing in the fragmentation region of this isolated quark occur via a cascade of pairs produced from the vacuum as shown in Fig. 1[3]. These hadrons are produced in a multi-peripheral-like chain with each meson generation coming from a quark q_i combining with a pair $\bar{q}_j q_j$, forming a meson $m = (q_i \bar{q}_j)$ and leaving a new quark q_j. This process repeats itself until a quark finally finds itself in the central region where it recombines with the other quarks originating from the initial target particle.

(3) The probability of finding a quark $\bar{q}_j$ is independent of the identity of q_i. This is assumed to be due to the interaction being a "color" interaction, whereas the indices j and i are "flavor" indices. We take for these probabilities:

$\bar{q}_j$	Probability
$\bar{u}$	.4
$\bar{d}$	.4
$\bar{s}$	.2

where higher-mass quarks are ignored. The justification for these numbers is given in Ref. 1; the smaller value for a strange quark is presumably due to its larger mass.

(4) A pair $(q_i\bar{q}_j)$ will yield a meson m with quantum numbers given by the quarks. We assume that mesons produced in this fashion lie wholly in the lowest-mass multiplet possible. Thus, if the $q_i\bar{q}_j$ helicities are opposite, we choose m to be a pseudoscalar meson; if the helicities are the same, we choose m to be a vector meson. This gives a vector to pseudoscalar ratio = 1. When several mesons in the multiplet contain $(q_i\bar{q}_j)$ the meson production probabilities are given by the appropriate SU(3) Clebsch-Gordon coefficients. For example, for mesons produced from a u quark, this process yields the following table[1]:

Pseudoscalar	Probability	Vector	Probability
π^+	.2	ρ^+	.2
π^o	.1	ρ^o	.1
η^o	.05	ω^o	.1
η'	.05	ϕ^o	.0
K^+	.1	K^{+*}	.1

The probability to produce a meson m from a quark q_i is called $C_m^{q_i}$, with $\sum_m C_m^{q_i} = 1$. Note that the production of baryons and heavy mesons is assumed to be small and is therefore ignored.

(5) In the process $q_i \to m + q_j$, where $m = (q_i\bar{q}_j)$, the energy of the initial quark is shared by the final meson and quark. In the high energy limit, this happens in a scale invariant manner; that is, the probability of finding a given value of E_m depends only on $E_m/E_{q_i} = z_i$. The distribution in z_i is then specified by a function for each meson. We shall assume that this function, $f(z_i)$, which we call the energy sharing function, is independent of q_i and q_j. Thus, the probability of getting a meson m, with fractional energy z_i, at each step is given by $C_m^{q_i} f(z_i)$. We make the simple choice $f(z_i) = 1$, for $0 \leq z_i \leq 1$. Thus, on the average, m and q_j each wind up with half the energy of the quark q_i.

These production probabilities can be used in a Monte Carlo computer program to generate leading particle spectra for given initial quark configurations. Figure 2[1] shows a comparison of the model with inclusive distributions seen in neutrino scattering. These distributions, called $zD_u^{\pi^+}(z)$ and $zD_u^{\pi^-}(z)$, are most cleanly measured in the neutrino processes, since the parent quark's identity is known to very good accuracy, and there is no diffractive production at large $z = E_{hadron}/E_{max}$. The hadron charge chosen in Fig. 2 avoids the necessity for corrections for proton and K^+ admixtures in the data. The agreement is very good for $z \gtrsim .3$, which is the region where scale-invariant fragmentation might be correct at these energies.

In the following sections, distributions are presented in terms of various momentum and energy variables. The fractional longitudinal momentum variable used will be x_F, equal to the longitudinal momentum divided by its maximum possible value in the appropriate center of mass reference frame. The initially scattered quark starts out with $x_F = 1$ in this frame. In the high energy limit $x_F \simeq z$ for forward going particles. In subsequent sections, we shall typically ignore the difference between these two variables and often use x_F since it provides a better separation of the various fragmentation regions for lepton scattering processes.

II. TRANSVERSE MOMENTUM

To date, there is little detailed understanding of the nature of transverse momentum in the quark-parton model-- in fact, transverse momentum is typically ignored, as in the calculation for Fig. 2. We shall now take it into account in a phenomenological way using data from muon-proton and pion-proton scattering as a guideline as described below. The principal results used are as follows[4,5,6]:

(1) Distributions in transverse momentum for leading particles (defined to be all those that have a fractional longitudinal momentum $x_F \geq 0.3$) can be described by a simple exponential $\frac{dN}{dp_\perp^2} \sim e^{-Bp_\perp^2}$, for $p_\perp \lesssim 1$ GeV/c. The value of B is approximately the same for all vector and pseudoscalar mesons for large x_F[4,6].

(2) For particles other than pions, B is approximately independent of x_F[6]. For pions, the average $p_\perp$ is smaller at low x_F values; however, since many pions in this region may be decay products of other mesons, this may not be a reflection of what happens for "directly" produced pions.

Based on these results, we take the transverse momentum distribution for $p_\perp \lesssim 1$ GeV/c, for all directly produced mesons, at all x_F, to be given by $\frac{dN}{dp_\perp^2} \sim e^{-Bp_\perp^2}$ where B depends only on the center-of-mass energy. The value of B can then be taken directly from data for leading pions. In the Monte Carlo quark dressing program, the transverse momentum of each meson is generated independently, using the exponential formula above, once B has been determined.

The result of including such a transverse momentum distribution in the quark dressing calculations can be displayed in several ways. For this purpose, we compare first with the inelastic muon scattering results of Ref. 4. For the center-of-mass energy region of this experiment, $W \simeq 3.5$ GeV, $B \simeq 4.5$[4,5]. For definiteness, the initial quark population in the calculation is assumed to come

from the "sea" quarks of the proton. The results are, however, nearly independent of the initial quark mixture chosen, for any reasonable choice.

Fig. 3 shows the transverse momentum distribution for all negative particles materializing in the direction of the virtual quark ($x_F>0$) produced in the final state of the muon-proton scattering process. The dashed curve shows the result of the model calculation with a vector to pseudoscalar ratio of one, as discussed in the introduction. The solid curve is the direct pion contribution which comprises about 20% of the total number of pions. Thus, the low mass meson resonances decaying to pions account quite accurately for the steepening seen at small $p_\perp$.

The above comparison is independent of the choice for the energy sharing function. To include this feature, we need to show how the transverse momentum is correlated with x_F. Fig. 4 shows $\langle p_\perp \rangle$ vs x_F for the same data sample used in the previous figure. Again, the agreement with the model is quite good, with the steeper $p_\perp$ distribution at small x_F now showing up as a dip in the $\langle p_\perp \rangle$ at small x_F.

Finally, we can look at the energy dependence of the $\langle p_\perp \rangle$[7]. We break the data into a high $-x_F$ ($x_F \simeq .6$) and low $-x_F$ ($x_F \simeq .15$) bin. The large x_F region serves to determine the slope parameter B and the low x_F region provides the test of the model. The results are shown in Fig. 5. Again, the agreement is quite good.

The quark dressing model therefore gives a good phenomenological account of all of the transverse momentum data presented, and leads to several interesting conclusions about such distributions. First, the $\langle p_\perp \rangle$ for a directly produced pion is not smaller than for the heavier vector mesons, such as the ρ^0; it only appears smaller when indirect pions from resonance decay are included. Second, the $\langle p_\perp \rangle$ for all direct mesons is $\sim$500 MeV/c (upper curve in Fig. 6), and not $\sim$350 MeV/c (lower curve). Finally, the $\langle p_\perp \rangle$ in a direct production step is increasing somewhat more rapidly with the center-of-mass energy (upper curve in Fig. 6) than the overall $\langle p_\perp \rangle$ for pions, which is dominated

by the low x_F region. This is because pions from resonance decay share the increase among several particles, giving a slower apparent rate of increase.

III. SENSITIVITY TO ASSUMPTIONS

In this section we briefly explore the sensitivity to the model assumptions of the comparisons in Figs. 2 through 5. We initially assume that the energy sharing function is correct, and allow the vector to pseudoscalar ratio to vary. Turning first to Fig. 2, we can get a rough understanding of the fractional energy distributions at large z by making the following approximations:

a) Ignore the twenty percent strange particle contribution;

b) Take only the largest contributors to the distribution at large z. These are the first and second generation direct pion contributions and the first generation ρ contributions. Keeping only these contributions and using the coefficients from the table for u quark dressing, we obtain for large z:

$$D_u^{\pi^-}(z) \simeq (C_{\pi^0} + C_{\rho^0}) \log \left(\frac{1}{z}\right).$$

$$D_u^{\pi^+}(z) \simeq C_{\pi^+} + (C_{\rho^+} + C_{\pi^0} + C_{\rho^0}) \log \left(\frac{1}{z}\right).$$

Defining r = vector to pseudoscalar ratio:

$$C_{\pi^0} + C_{\rho^0} = .2,\ C_{\pi^+} = \frac{.4}{1+r}\ ,\ C_{\rho^+} + \frac{.4r}{1+r}.$$

Using also $\log \left(\frac{1}{z}\right) \simeq (1-z)$, for large z, gives finally:

$$D_u^{\pi^-}(z) \simeq .2(1-z)$$

$$D_u^{\pi^+}(z) \simeq \left(\frac{.4}{1+r}\right) + \left[\left(\frac{.4r}{1+r}\right) + .2\right] (1-z).$$

The agreement of the calculated $D_u^{\pi^-}(z)$ with the data is seen to be insensitive to the value of r; it therefore serves as a good test of the general approach. The data for $D_u^{\pi^+}$ serve to set a limit on r. In particular, r must be $\gtrsim 1$ to get agreement with the value of $D_u^{\pi^+}$ as $z \to 1$. Taking $r = 3$, the value expected for SU(6) invariance, would, however, give nearly as good agreement with the data as $r = 1$[1]. The errors on the measured distributions are therefore too large to provide a very stringent limit on r. Note, that $D_u^{\pi^+}/D_u^{\pi^-} \geq 3$ at large z for any value of r.

Turning now to the transverse momentum distributions, we find that it is also difficult in this case to determine r accurately since so few pions are directly produced if $r \geq 1$. For example, taking $r = 3$ instead of 1 changes the number of direct pions from 20% to 10% of the total, and changes the predicted curves in Figs. 3 through 5 by typically less than 10% everywhere.

We can conclude therefore that the inclusive pion distributions provide weak limits on r, and that it is particularly important to directly measure the inclusive meson cross sections in order to justify the assumptions used in fragmentation calculations, and also to provide a more incisive comparison of the final states seen in different inelastic processes. For example, the easiest cross section to measure might be that of the ρ^o meson for which we predict for $r = 1$:

$$\frac{z}{\sigma_{tot}} \frac{d\sigma^{\rho^o}}{dz} \simeq .08.$$

Fig. 6 shows a comparison of this distribution with the inclusive ρ^o cross section seen in photoproduction[8]. Although this is not necessarily thought of as a highly inelastic process, the data agree quite well with the prediction.

The principal justification of the energy sharing function has been the comparisons in Fig. 2. Considering only directly produced mesons, and summing over meson types and many quark generations, our model gives an inclusive distribution, which is flat:

$$\sum_m \frac{z}{\sigma_{tot}} \frac{d\sigma^m}{dz} = 1.$$

The rise of the pion distributions at small z comes about because of the subsequent decay of resonances. An alternative approach, with various theoretical justifications[9], would be to assume that $f(z_i)$ falls with increasing z_i. This might then give the observed rise, provided that resonance contributions are small enough. A numerical comparison of these two alternatives can be found in Ref. 1; again, a direct measurement of the various meson cross sections would help considerably in choosing among these alternatives.

IV. CORRELATIONS IN HIGH TRANSVERSE MOMENTUM FINAL STATES

A. Introductory Remarks on Pion Triggered Jets

We consider in this section the process $p + p \to \pi^{trig} +$ hadrons, where the measurements are made in an experiment triggering on a high transverse momentum π at 90° in the p - p center of mass. We assume that the π^{trig} comes from the dressing of a quark scattered out to large $p_\perp$, as, for example, in the model of Field and Feynman[10]. Our quark dressing model already agrees with the different meson ratios at high transverse momentum; indeed, these ratios provided the principal experimental justification for the coefficients C_m^{qi} in Ref. 1. Since we can generate several meson generations, yielding a full jet of particles, we will focus here instead on the particles in the jet accompanying a trigger particle of given type.

In order to proceed, we assume, for the case of a pion trigger:

(1) The scattered quark in the final state is chosen from the valence quarks of the proton giving a 2/3 probability to find a u quark, 1/3 a d quark. The actual results presented are, however, nearly independent of the assumed parent quark mixture.

(2) In order to correctly match the measured pion distributions[11] at high transverse momentum, we take for the parent quark energy distribution at a 90° scattering angle:

$$\frac{dN}{dE^2} \sim \frac{1}{(1+E^2)^4} \quad (1-x_\perp)^9, \text{ where } x_\perp = \frac{2E}{\sqrt{s}}, \text{ and E is the quark energy.}$$

(3) Mesons are generated from the initial quark along its production direction using the model outlined in the introduction; the momentum transverse to the quark direction was generated exponentially with a slope parameter B = 4.5 (see Section II).

To evaluate the uncertainty due to the above, we have first recalculated our results using another successful parametrization of the initial quark distribution[12]:

$$\frac{dN}{dE^2} \sim \frac{1}{(1 + E^2)^4} \; e^{-13x_\perp} ;$$

and, secondly, for a slope parameter B = 3.5[6]. These changes in parametrization affect the calculated results by 15% and 5%, respectively. We take this as an indication that all the results presented in the next sections have an intrinsic uncertainty of about 20% due to the uncertainties in assumptions (2) and (3) above.

1. π^o Trigger

For our comparison we use the data of Ref. 13 from the ISR. To make a quantitive test we have included in the Monte Carlo quark dressing calculation:

(1) The π^o acceptance of that particular experiment.

(2) The angular cuts for accepting charged tracks.

(3) The experimental resolution in mass reconstruction for particles originating from ρ^+ or ρ^- mesons.

The results are shown in Fig. 7, where the particle density per event for charged particles accompanying a π^o of $2.0 \leq p_\perp^{\pi^o} \leq 4.1$ is displayed. The distributions shown are binned in the usual center of mass longitudinal rapidity, y, and the invariant $\pi^o\pi^\pm$ mass for four regions of the transverse momentum component of the charged track, p_x, along the π^o direction. Uncorrelated tracks from the "non-jet" part of the event, called the minimum-bias distribution[13], are shown as the dashed background, to which the correlated part is added. The trigger π^o carries on the average .85 of the initial quark's energy.

The results of the Monte Carlo calculation indicate that 48% of the correlated tracks seen in this experiment come from a ρ^+ or ρ^- which yielded also the trigger π^o. They produce the peaks in the rapidity distribution at $|y| \approx .5$

for low p_x. These peaks are not obvious in the data which are presented in large bins in y. In the mass distribution, the ρ^+ and ρ^- contribution are obscured except at large p_x, a feature faithfully reproduced by the Monte Carlo calculation. The calculations provide a good representation of the experimental results.

2. π^+ and π^- Trigger

In a similar manner, we predict the distributions expected in an experiment triggering now on charged pions at 90° for a center-of-mass energy = 53 GeV at the ISR. The results, displayed in Fig. 8, are the charged particle density per event, per unit p_x, accompanying a triggering charged pion with transverse momentum either between $2 \leq p_\perp^{trig} \leq 3$GeV/c or between $3 \leq p_\perp^{trig} \leq 4$GeV/c. The transverse momentum component of the accompanying track along the trigger pion's momentum is defined as p_x; it is further assumed that the trigger efficiency has been divided out if dependent on $p_\perp^{trig}$, and that the minimum bias background has been subtracted out. The results are shown for a p_x range $.4 \leq p_x \leq 1.5$ GeV/c; the distributions are approximately exponential in shape over this region. The correlated tracks in this region come 38% of the time from a ρ^o which yields simultaneously the trigger pion. Although the distributions shown in Fig.7 are very convenient for pointing out jet-like features, once these are established, it is useful to plot $\frac{dN}{dp_x}$ as in Fig. 8. This distribution by straight forward integration can yield the correlated multiplicity or the average transverse momentum carried by the correlated tracks. The latter quantity, when compared with $p_\perp^{trig}$, can serve to test the shape of the energy sharing function near $z = 1$.

The use of a charged pion trigger allows a good test of the model based on the charge correlation between the trigger particle and the other particles in the jet. This correlation comes about because of the presence of meson decays

which provide the trigger particle, very predominantly the ρ^o in the present case, and because the charge correlation of the $q\bar{q}$ chain is partially passed on to the mesons generated, as illustrated by the data in Fig. 2. Both of these effects are important. Taking all events triggered on charged pions of $3 \leq p_{\perp}^{trig} \leq 5$ GeV/c, the Monte Carlo calculation gives a ratio of 5.5 to 6.0 for the probability of finding an accompanying particle of opposite charge to the trigger to that for a particle of the same sign charge (after subtraction of the minimum bias background) for any p_x value between .4 and 1.5 GeV/c. It is important that the data used to calculate this ratio come from an experiment with nearly full acceptance since the various components making up the ratio have different opening angle distributions relative to the trigger particle, an effect seen earlier in Fig. 7. The large value of this ratio should provide a useful test of the model used.

B. Charged Kaon Triggered Jets

The distributions accompanying a charged kaon trigger particle are somewhat more difficult to predict than those for a pion trigger because of the greater role of the "sea" quarks in the incident proton. The strange particle component in the sea and the size of the sea versus valence part are not accurately known. For $x_\perp \simeq .1$, typical of ISR data for $\sqrt{s}$ = 53 GeV, we can, however, expect the sea and valence parts to be about equal. Based on the particle ratios[14] seen at $x_\perp \simeq .1$, we take the quark parentage at $x_\perp = .1$ to be given by the following table.

Quark Type	Contribution		
	Valence	Sea	Total
u	2	1	3
$\bar{u}$	0	1	1
d	1	1	2
$\bar{d}$	0	1	1
s	0	½	½
$\bar{s}$	0	½	½

Note the strange quarks in the sea are assumed to be suppressed by the same factor of two as in the dressing calculation.

These quark parents yield trigger particle ratios of

$$\frac{\pi^+}{\pi^-} = 1.3, \quad \frac{K^+}{\pi^+} = .5, \quad \frac{K^-}{\pi^-} = .3,$$

all close to the values seen. A trigger on a K^+ leaves a different leftover first generation quark mixture than for a K^-, giving rise to small differences between these two trigger types. With the quark parent composition above these first generation quarks are approximately:

For K^+: 3/4 s and 1/4 $\bar{u}$;

For K^-: 1/2 $\bar{s}$ and 1/2 u .

Thus, both K^+ and K^- are expected to be accompanied sometimes by opposite sign kaons, with this occurring somewhat more frequently for the K^+. The frequent presence of a first generation leftover strange quark gives a smaller charged particle correlated component for a kaon trigger than a pion trigger because a strange quark dresses more frequently to a neutral meson than a u quark.

An additional effect which must be taken into account is that the sea quark to valence quark ratio drops with $x_\perp$, for $x_\perp > .1$. To take this into account quantitatively, the sea to valence ratio is assumed to drop like $(1-x_\perp)^2$ for $x_\perp > .1$. For $x_\perp$ near .1, this has only a small effect on the correlated particle density accompanying a kaon trigger particle so that the results presented here are not very sensitive to the function chosen above.

With the assumptions outlined, the Monte Carlo program can be used to generate kaon triggered events at 90° for $\sqrt{s} = 53$ GeV. We calculate again $\frac{dN}{dp_x}$ for associated charged particles after the subtraction of the minimum bias distribution. The principal results, good to about 10% accuracy, for the kinematic range $2. < p_\perp^{\text{trig}} < 4.$ GeV/c, and $.4 \leq p_x \leq 1.5$ GeV/c, are as follows:

(1) $\left(\frac{dN}{dp_x}\right)_{K^+ \text{ trigger}} \simeq \left(\frac{dN}{dp_x}\right)_{K^- \text{ trigger}}$.

(2) $\left(\frac{dN}{dp_x}\right)_{K^+ \text{ trigger}} \simeq .75 \left(\frac{dN}{dp_x}\right)_{\pi^\pm \text{ trigger}}$

(3) The particles making up the correlated component contain:

18% K^- for a K^+ trigger,

15% K^+ for a K^- trigger,

6% K^+ plus K^- for a $\pi^\pm$ trigger.

(4) The above features are nearly independent of p_x and $p_\perp^{\text{trig}}$ for the range considered.

V. CONCLUSIONS

We have presented model calculations and comparisons of distributions for hadrons seen in several highly inelastic processes. Using particle ratios and transverse momenta typical of the final states in pion-proton scattering[6], we get a good description of the distributions seen. This may indicate that the dynamics in all of these processes are quite similar if leading particle effects could be properly allowed for. The comparison in Fig. 6 also seems to point in this direction.

Finally, we have predicted momentum distributions, the charge correlation ratio, and the kaon content in high transverse momentum quark jets leading to a triggering charged meson at 90° in the center of mass. A measurement of the predicted distributions should soon be available from experiments at the ISR, allowing a test of the origin of such jets.

REFERENCES

1. A. Seiden, SLAC-PUB-1837 (1976).

2. R.P. Feynman, Photon-Hadron Interactions (W.A. Benjamin, Reading, MA, 1972).

3. J. Kogut, Phys. Rev. D8, 3029 (1973).

4. C. del Papa et al., Phys. Rev. D15, 2425 (1977).

5. J.T. Dakin et al., Phys. Rev. D10, 1401 (1974).

6. P.K. Malhotra, CERN/EP/PHYS 76-46.
   P.K. Malhotra, CERN/EP/PHYS 76-47.
   M. Deutschmann et al., Nucl. Phys. B103, 426 (1976).

7. H.L. Anderson et al., Phys. Rev. Lett. 36, 1422 (1976).

8. E. Kogan et al., SLAC-PUB-1857 (1976).

9. G.R. Farrar and D.R Jackson, Phys. Rev. Lett. 35, 1416 (1975).
   L.S. Osborne, Phys. Lett. 63B, 456 (1976).

10. R.D. Field and R.P. Feynman, Cal Tech preprint CALT-68-565 (1976).

11. D. Antreasyan et al., Phys. Rev. Lett. 38, 112 (1977).

12. B. Alper et al., Nucl. Phys. B87, 19 (1975).
    F.W. Büsser et al., Nucl. Phys. B106, 1 (1976).

13. P. Darriulat et al., Nucl. Phys. B107, 429 (1976).

14. B. Alper et al., Nucl. Phys. B100, 237 (1975).

FIGURE CAPTIONS

1. Picture of meson production resulting from a quark, q_1, initially isolated in phase space. Mesons produced are m_1, m_2..., with the chain ending when an n^{th} generation quark finds itself locally near the other quarks which were isolated by the highly inelastic process.

2. Comparison of neutrino data and predictions for the quark fragmentation functions $zD_u^{\pi^+}(z)$ (closed circles) and $zD_u^{\pi^-}(z)$ (open circles). For further details, see Ref. 1.

3. Distribution in transverse momentum squared for all negative particles with $x_F > 0$ seen in the muon proton scattering experiment of Ref. 4. Average $Q^2 = 1$, average $W = 3.5$ for the data. Dashed curve is the model prediction for pions, using a transverse momentum slope parameter = 4.5, which is the typical slope for particles with large x_F [4,5] at this center of mass energy. Solid curve is the direct pion contribution, which amounts to 20% of the total.

4. $\langle p_\perp \rangle$ versus x_F for the data in Fig. 3, now broken into different Q^2 bins. The solid curve is the model prediction.

5. $\langle p_\perp \rangle$ for two x_F values versus center of mass energy. The open points determine the slope parameter B and the solid points provide a test of the model (solid lines). The circles are from Ref. 4, squares are average of several points from Ref. 5, and the triangles are from Ref. 7 at the estimated average center of mass energy of that experiment.

6. Inclusive ρ^o production in photon-proton scattering from Ref. 8. Dashed curve is the model prediction if we assume that it applies to photoproduction. For x_F near 1, deviations at higher energies might be expected as diffractive states, not included in the model, begin contributing more strongly.

7. Correlated charged particle density accompanying a high transverse momentum π^0. The correlated particles are grouped into four p_x bins and are plotted in terms of their center of mass longitudinal rapidity and invariant mass with the triggering π^0. The dashed curves are the measured minimum bias backgrounds to which the model predictions have been added, giving the solid curves.

8. Correlated charged particle density, per event, expected for a 90° charged pion trigger. The predicted density is approximately given by $.5e^{-Ap_x}$ for $.4 < p_x < 1.5$ GeV/c, with A values:

$$A = 2.5 \quad \text{for} \quad 2 < p_\perp^{trig} < 3$$

$$A = 2.0 \quad \text{for} \quad 3 < p_\perp^{trig} < 4 \ .$$

For p_x values smaller than .4 Gev/c, the distribution should depend strongly on the quark-recombination mechanism in the central region and it may therefore deviate considerably from the curves shown. It is assumed that the minimum bias background has been subtracted before plotting the distributions.

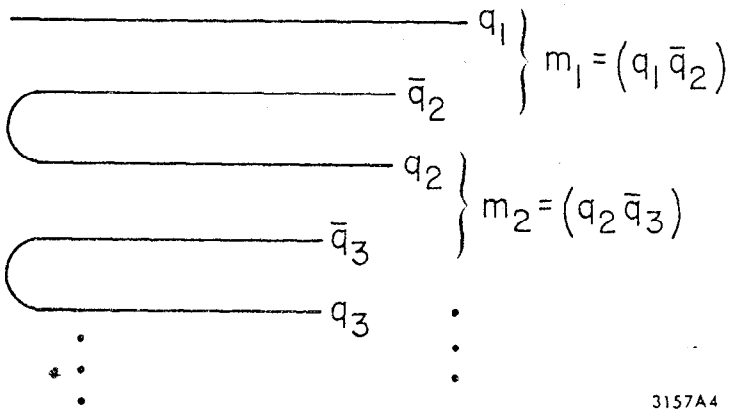

Fig. 1

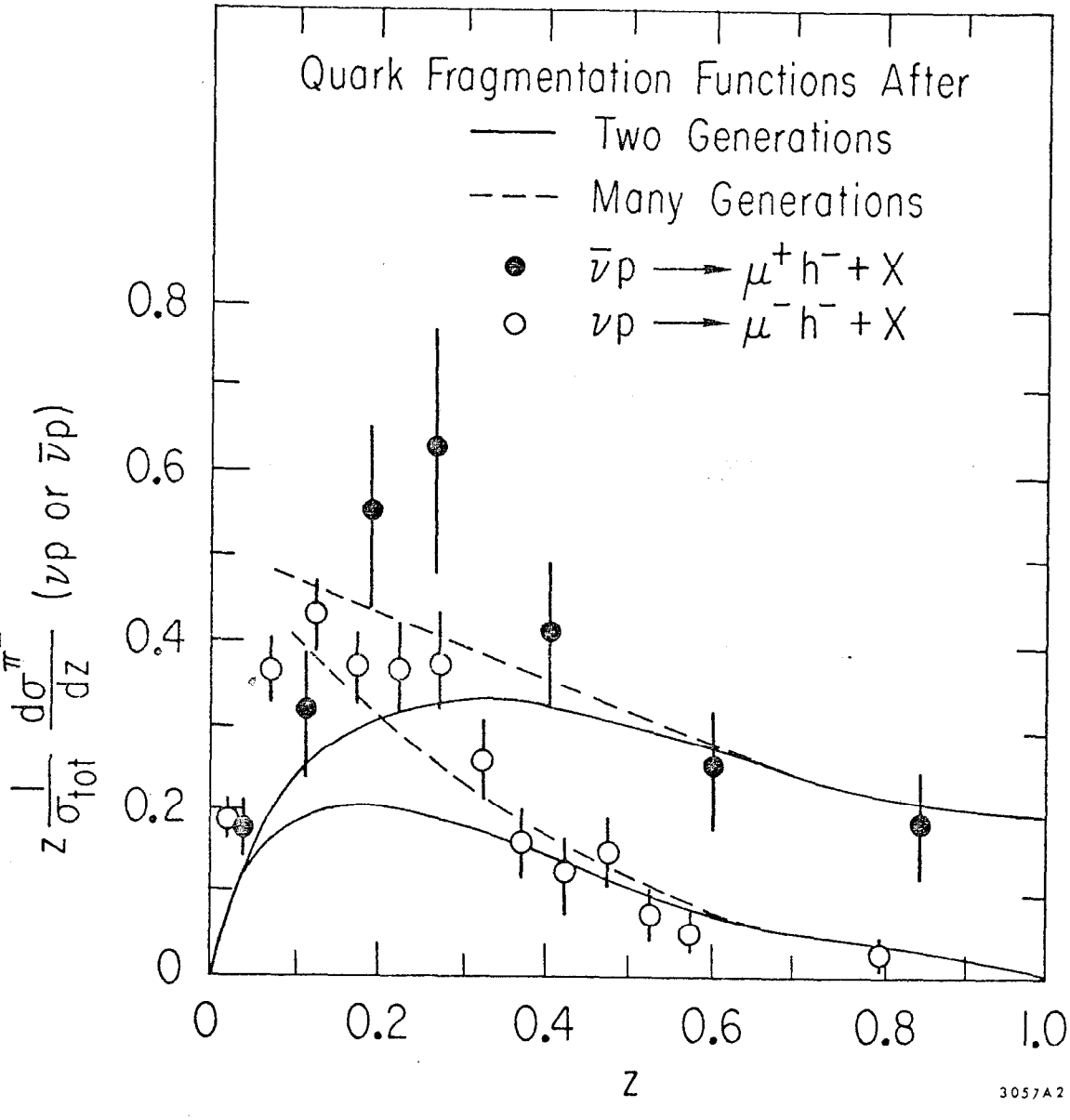
Quark Fragmentation Functions After
Two Generations
Many Generations
$\bar{\nu}p \longrightarrow \mu^+ h^- + X$
$\nu p \longrightarrow \mu^- h^- + X$
$\frac{1}{\sigma_{tot}} \frac{d\sigma^{\pi^-}}{dz}$ (νp or $\bar{\nu}p$)
0
0.2
0.4
0.6
0.8
1.0
z
3057A2

Fig 2

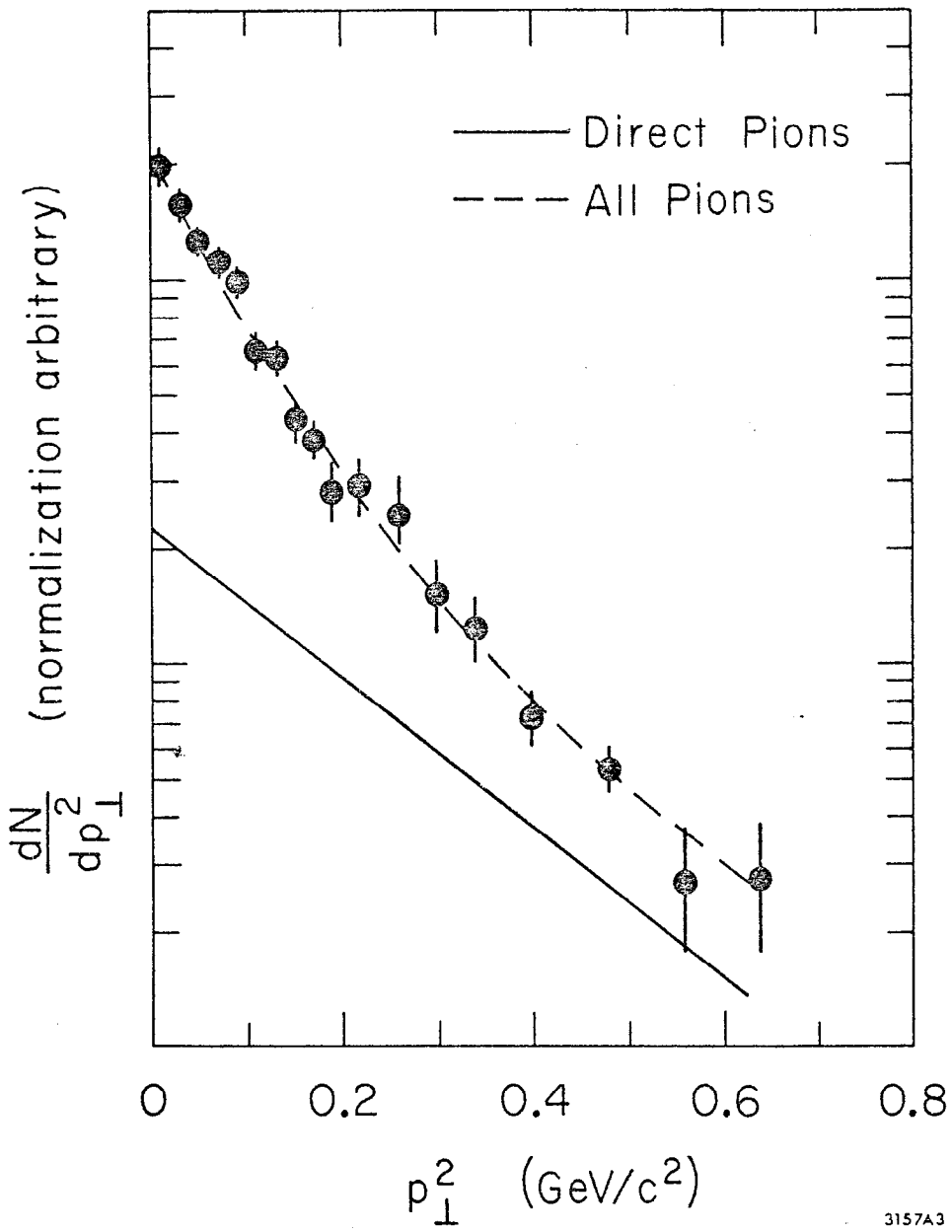
Direct Pions
All Pions
$\frac{dN}{dp_\perp^2}$ (normalization arbitrary)
0
0.2
0.4
0.6
0.8
$p_\perp^2$ (GeV/c^2)
3157A3

Fig 3

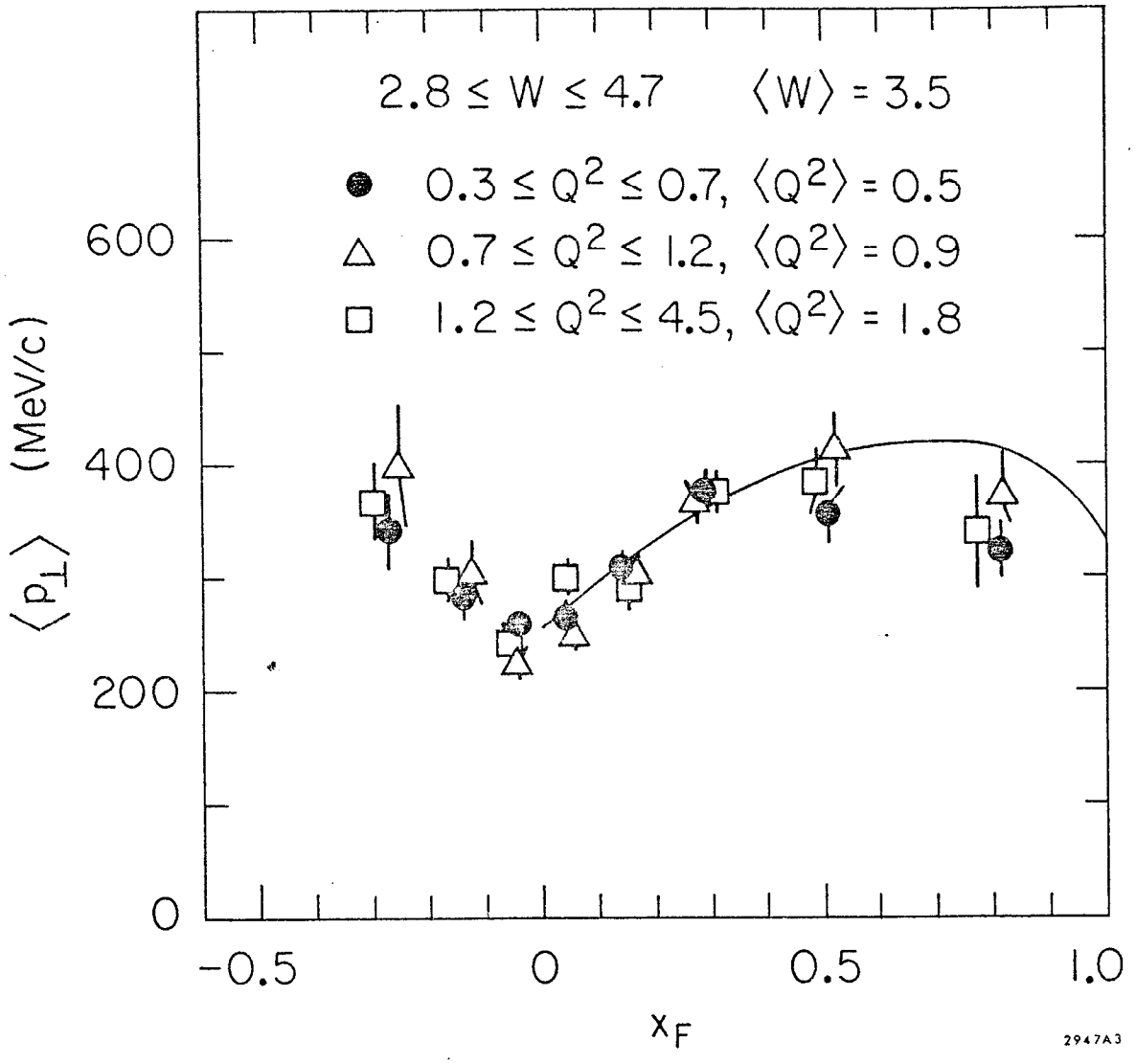
2.8 ≤ W ≤ 4.7 ⟨W⟩ = 3.5
0.3 ≤ Q² ≤ 0.7, ⟨Q²⟩ = 0.5
0.7 ≤ Q² ≤ 1.2, ⟨Q²⟩ = 0.9
1.2 ≤ Q² ≤ 4.5, ⟨Q²⟩ = 1.8
⟨pT⟩ (MeV/c)
600
400
200
0
-0.5
0
0.5
1.0
xF
2947A3

Fig. 4

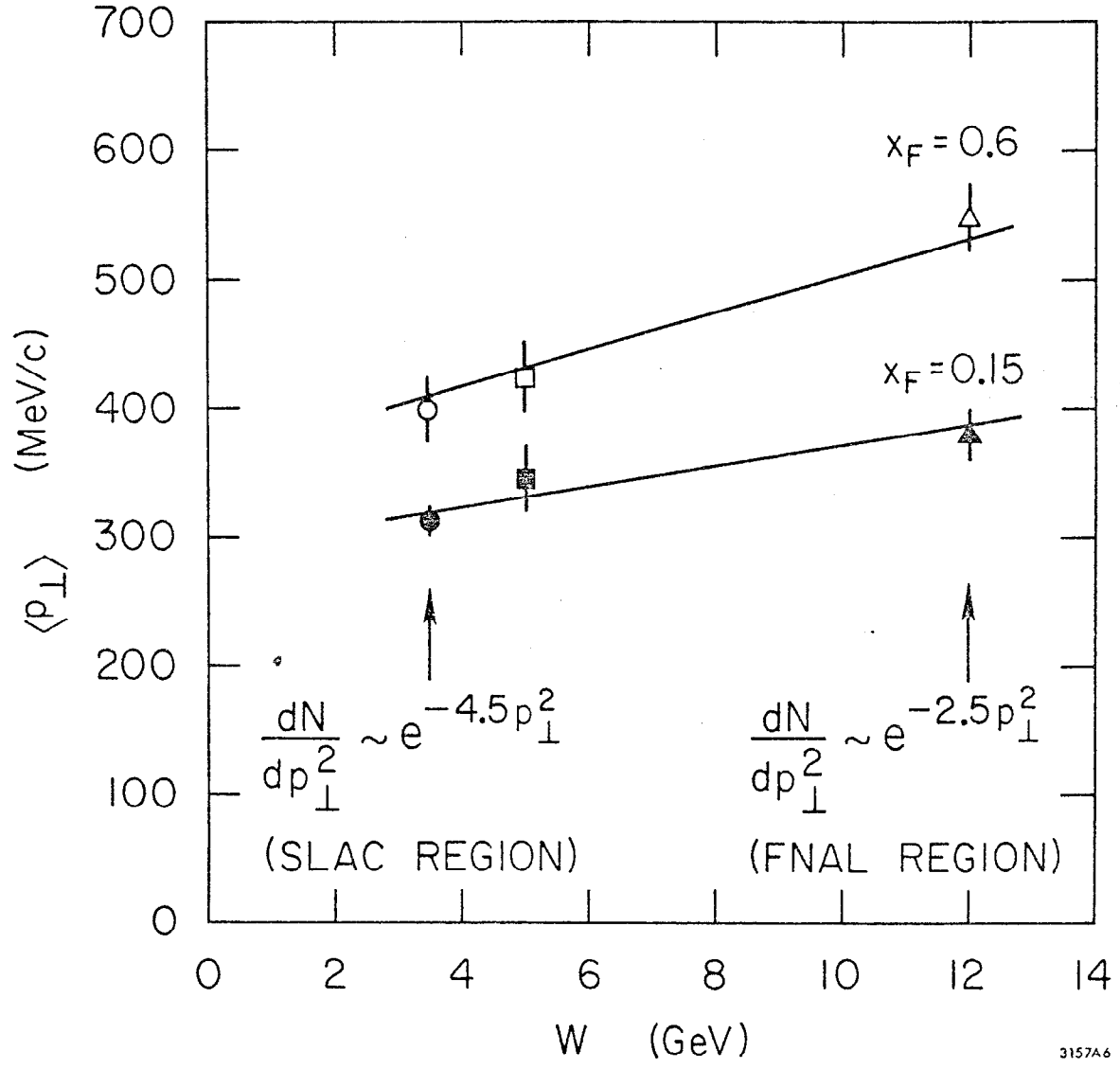
700
600
500
400
300
200
100
0
$\langle p_\perp \rangle$ (MeV/c)
$x_F = 0.6$
$x_F = 0.15$
$\frac{dN}{dp_\perp^2} \sim e^{-4.5p_\perp^2}$
$\frac{dN}{dp_\perp^2} \sim e^{-2.5p_\perp^2}$
(SLAC REGION)
(FNAL REGION)
0
2
4
6
8
10
12
14
W (GeV)
3157A6

Fig. 5

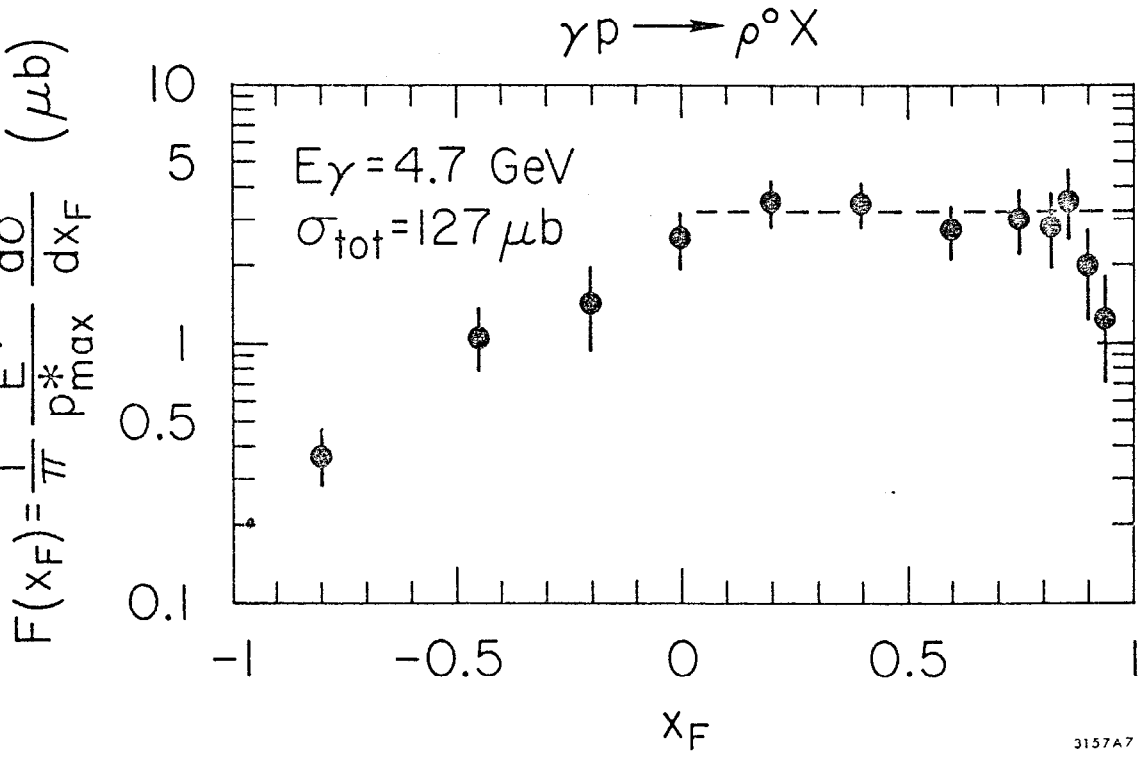
γp ⟶ ρ°X
Eγ = 4.7 GeV
σtot = 127 μb
F(xF) = 1/π E*/p*max dσ/dxF (μb)
10
5
1
0.5
0.1
-1
-0.5
0
0.5
1
xF
3157A7

Fig. 6

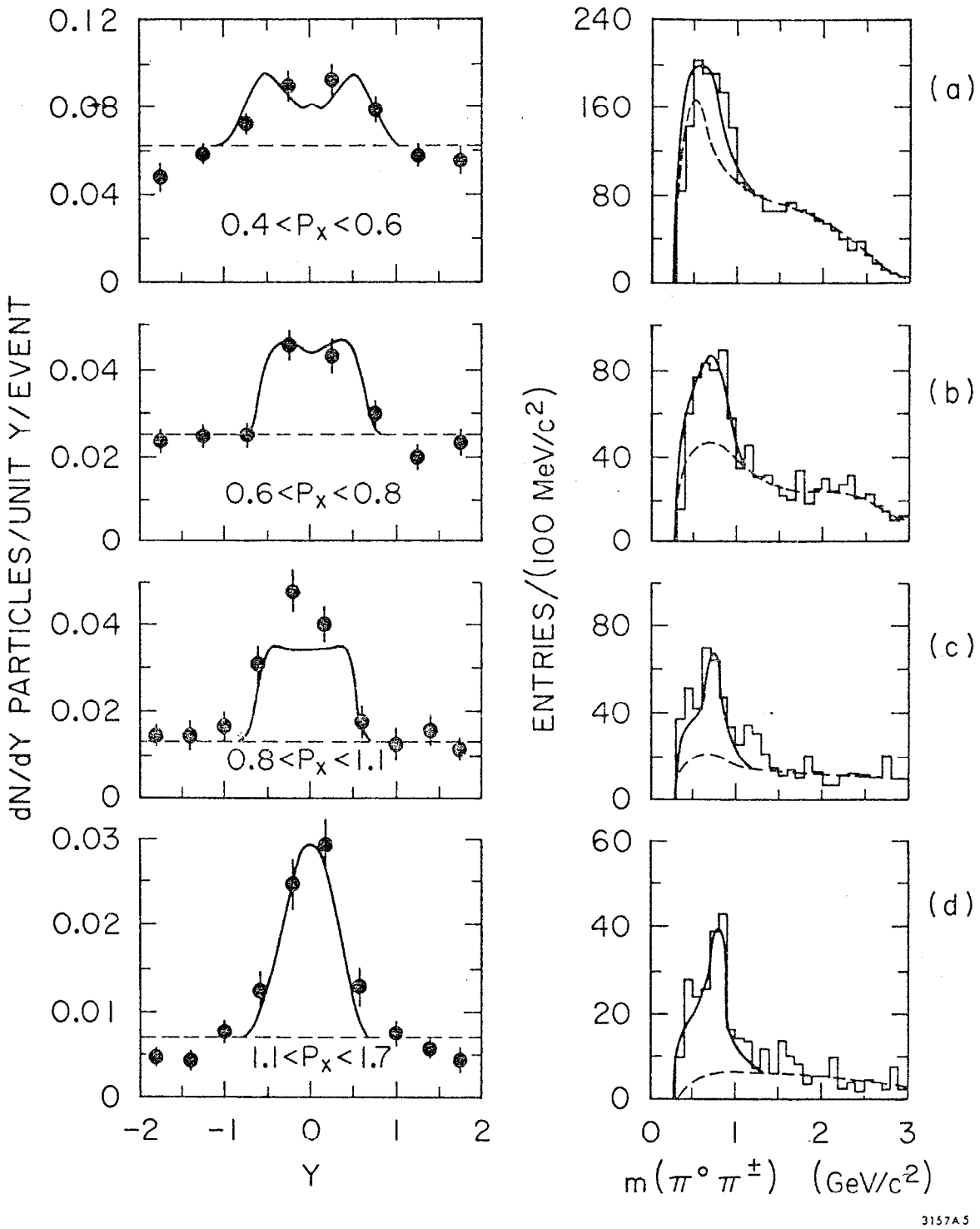
0.12
0.08
0.04
0
0.4<Px<0.6
0.04
0.02
0
0.6<Px<0.8
0.04
0.02
0
0.8<Px<1.1
0.03
0.02
0.01
0
1.1<Px<1.7
-2
-1
0
1
2
Y
dN/dY PARTICLES/UNIT Y/EVENT
240
160
80
0
(a)
80
40
0
(b)
80
40
0
(c)
60
40
20
0
(d)
0
1
2
3
m(π° π±) (GeV/c2)
ENTRIES/(100 MeV/c2)
3157A5

Fig. 7

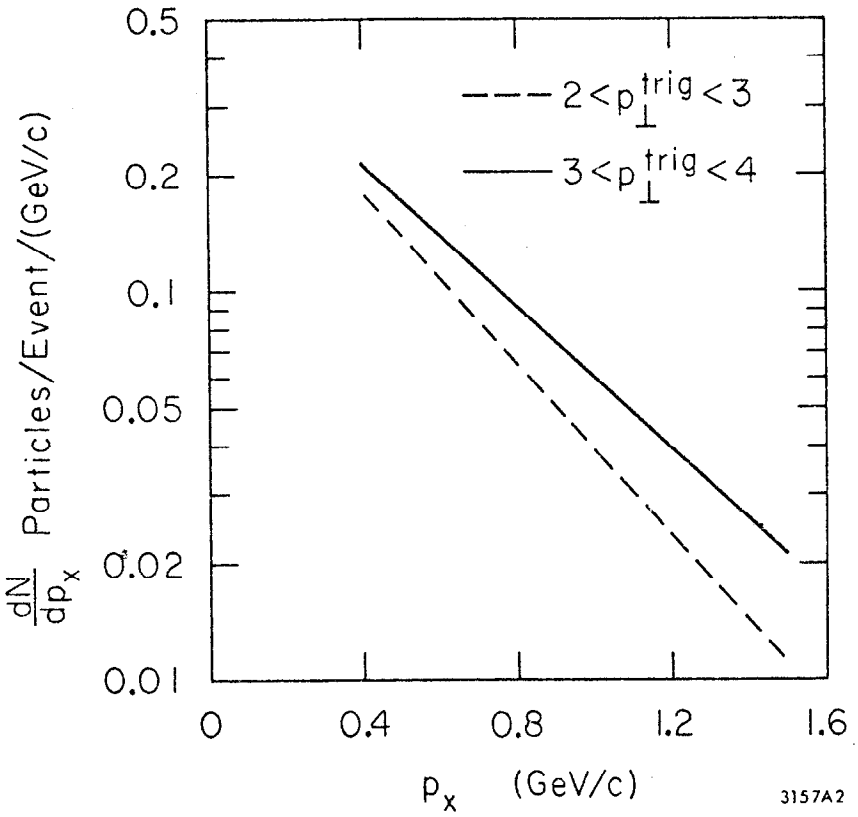
0.5
0.2
0.1
0.05
0.02
0.01
0
0.4
0.8
1.2
1.6
$\frac{dN}{dp_x}$ Particles/Event/(GeV/c)
p_x (GeV/c)
$2<p_\perp^{trig}<3$
$3<p_\perp^{trig}<4$
3157A2

Fig. 8